Synthesis, Structural Characterization, Magnetic Properties, and Ionic Conductivity of $Na_4M^{II}_3(PO_4)_2(P_2O_7)$ (M^{II} = Mn, Co, Ni)

F. Sanz,[†] C. Parada,[‡] J. M. Rojo,[†] and C. Ruíz-Valero*,[†]

Instituto de Ciencia de Materiales de Madrid, CSIC, Cantoblanco, E-28049 Madrid, Spain, and Departamento de Química Inorgánica, Facultad de C. Químicas, Universidad Complutense, E-28040 Madrid, Spain

Received October 25, 2000

The new phases, $Na_4M_3(PO_4)_2(P_2O_7)$ (M = Mn, Co, Ni), have been synthesized by solid-state reactions. Single crystals of $Na_4M_3(PO_4)_2(P_2O_7)$ (M = Mn, Ni) have been isolated and their structure has been determined by X-ray diffraction techniques using as the starting model the structure of the isostructural compound $Na_4Co_3(PO_4)_2(P_2O_7)$. These compounds crystallize in the orthorhombic noncentrosymmetric space group $Pn2_1a$ with a = 17.991(3) Å, b = 6.6483(1), and c = 10.765(2) Å for the manganese compound and a = 17.999(2), b = 6.4986(6) Å, and c = 10.4200(9) Å for the nickel compound, with Z = 4. Magnetic measurements reveal the existence of antiferromagnetic interactions in the nickel compound. The manganese and cobalt compounds show canting antiferromagnetic behavior at low temperatures. Magnetic correlation is also studied from the analysis of possible superexchange pathways in the structure. The ionic conductivity, due to Na^+ ions, is measured for the three compounds. The activation energy is nearly the same (0.81−0.86 eV), but the conductivity at 300 °C changes, increasing from 2.1 × 10^{-7} S cm^{-1} for the Ni compound to 1.3 × 10^{-6} S cm^{-1} for the Co one, and then from this value to 2.7 × 10^{-5} S cm^{-1} for the Mn compound.

Introduction

Despite the great number of new structures of transition metal phosphates determined during the past years, only a limited number of phosphates show both PO_4 and P_2O_7 groups in their structure.[1] On these compounds we have reported[2,3] the crystal structures of two new mixed-anion phosphates with compositions $Na_4Co_3(PO_4)_2(P_2O_7)$ and $Na_4Ni_5(PO_4)_2(P_2O_7)_2$. It is worth noting that the two structures are quite similar, showing double chains, which are built up from MO_6 octahedra and PO_4 groups sharing corners. The double chains are formed of simple parallel chains running in the [010] direction. In both structures there are infinite blocks parallel to the *bc* plane, the blocks being linked through diphosphate groups. However, the main difference of the two structures is the presence of bioctahedral face-sharing units, Ni_2O_9, in the $Na_4Ni_5(PO_4)_2(P_2O_7)_2$ compound. The presence of these units gives rise to a less open framework in which tunnels are only observed along the *a* direction whereas in $Na_4Co_3(PO_4)_2(P_2O_7)$ the tunnels are extended along the three main crystallographic directions [100], [010], and [001].

In the phosphate field some of these compounds are obtained by classical reactions of aqueous chemistry, but the vast majority of them are prepared by using flux-method experiments.[1] It is very unusual to obtain the mixed-anion phosphates as microcrystalline powder through solid-state reactions.

Taking into account the structural features of these new phosphates, interesting physical properties could be expected. In this paper we present the synthesis, structural characterization, magnetic properties, and ionic conductivity of the phases $Na_4M_3(PO_4)_2(P_2O_7)$ (M = Mn, Co, Ni).

Experimental Section

Synthesis. Single crystals of $Na_4Co_3(PO_4)_2(P_2O_7)$ were grown as has been described in a previous report.[2] Of similar form, single crystals of $Na_4M_3(PO_4)_2(P_2O_7)$ (M = Mn, Ni) were grown by melting a mixture of analytical grade $Na_4P_2O_7$, $Mn(NO_3)_2{\cdot}6H_2O$ or $MnCO_3$, $Ni(NO_3)_2{\cdot}6H_2O$, and $NH_4H_2PO_4$, in the molar ratio Na/M/P = 4:3:4. After grinding, the mixtures were heated to 800 and 900 °C for the manganese and nickel compounds, respectively. The furnace was kept at these temperatures for 2 h to homogenize the melts, then being cooled to 400 °C at 10 °C/h. The samples were finally quenched to room temperature. At the end of the process, many prismatic single crystals of manganese and nickel, brown and yellow in color, respectively, were obtained on the surface of the cake melt.

The new phases, $Na_4M_3(PO_4)_2(P_2O_7)$ (M = Mn, Co, Ni), were also obtained as a microcrystalline powder by solid-state reaction, employing as precursors $Na_4P_2O_7$, $MnCO_3$, $CoCO_3{\cdot}4H_2O$, $Ni(NO_3)_2{\cdot}6H_2O$, and $NH_4H_2PO_4$, in the same molar ratios used to obtain single crystals. The mixtures were heated at 300 °C in a porcelain crucible to decompose and remove the volatile species. Then, accumulative treatments for 24 h each

* To whom correspondence should be addressed. E-mail: crvalero@icmm.csic.es. Telephone: +34 91 3349026. Fax: +34 91 3720623.
[†] CSIC.
[‡] Universidad Complutense.

(1) Durif, A. *Crystal Chemistry of Condensed Phosphates*; Plenum Press: New York, 1995.
(2) Sanz, F.; Parada, C.; Amador, U.; Monge, M. A.; Ruíz-Valero, C. *J. Solid State Chem.* **1996**, *123*, 129.
(3) Sanz, F.; Parada, C.; Rojo, J. M.; Ruíz-Valero, C. *Chem. Mater.* **1999**, *11*, 2673.

10.1021/cm001210d CCC: $20.00
Published on Web 03/15/2001

Table 1. Chemical Analysis of the $Na_4M_3(PO_4)_2(P_2O_7)$ (M = Mn, Co, Ni) Compounds (Calculated Data Are in Parentheses)

compound	% Na	% P	% M
$Na_4Mn_3(PO_4)_2(P_2O_7)$	14.10 (14.8)	19.5 (19.9)	25.9 (26.6)
$Na_4Co_3(PO_4)_2(P_2O_7)$	14.6 (14.5)	19.2 (19.5)	27.1 (27.9)
$Na_4Ni_3(PO_4)_2(P_2O_7)$	14.4 (14.5)	19.1 (19.6)	27.5 (27.9)

at 400, 500, 600, and 700 °C for manganese and cobalt samples and up to 800 °C in the case of the nickel sample were performed.

All the attempts to obtain these compounds in the case of Cu^{2+}, Zn^{2+}, and Cd^{2+} were fruitless.

Single-Crystal X-ray Diffraction. Two crystals of dimensions 0.08 × 0.04 × 0.02 and 0.16 × 0.04 × 0.09 mm for manganese and nickel compounds, respectively, were resin epoxy coated and mounted on a Siemens Smart CCD diffractometer equipped with a normal focus, 2.4-kW sealed tube X-ray source (Mo Kα radiation, $\lambda = 0.71073$ Å) operating at 50 kV and 40 mA. Data were collected over a hemisphere of reciprocal space by a combination of three sets of exposures. Each set had a different φ angle for the crystal and each exposure of 20 s covered 0.3° in ω. The crystal-to-detector distance was 6.01 cm. Coverage of the unique set was over 99% complete to at least 23° in θ. Unit cell dimensions were determined by a least-squares fit of 50 reflections with $I > 20\sigma(I)$ and $6° < 2\theta < 46°$. The first 30 frames of data were recollected at the end of the data collection to monitor crystal decay. The intensities were corrected for Lorentz and polarization effects. Scattering factors for neutral atoms and anomalous dispersion corrections for Mn, Ni, Na, and P were taken from the *International Tables for Crystallography*.[4] The structures of manganese and nickel compounds were solved using the structure of isostructural compound $Na_4Co_3(PO_4)_2(P_2O_7)$ as the starting model. The refinements were realized with (Mn, Ni, P, and Na) atom positions from the cobalt compound. The positions of the oxygen atoms were obtained by Fourier synthesis. The first stage of refinement was carried out with isotropic thermal parameters. Full matrix least-squares refinement with anisotropic thermal parameters for all the atoms was carried out by minimizing $w(F_o^2 - F_c^2)^2$. The maximum residual electron density was near the transition metal. Refinement on F^2 for all reflections, weighted R factors (R_w), and all goodnesses of fit S are based on F^2, while conventional R factors (R) are based on F. R factors based on F^2 are statistically about twice as large as those based on F, and R factors based on all data will be even larger.

All the calculations were performed using SMART software for data collection, SAINT[5] for data reduction, SHELXTL to refine the structure and to prepare material for publication,[6] and ATOMS[7] for molecular graphics.

Elemental Analysis. Chemical analysis in the powder samples was carried out on an I.C.P. (induced coupling plasma) apparatus. The observed data are in good agreement with the calculated data, as shown in Table 1.

X-ray Powder Diffraction. X-ray powder pattern of $Na_4M_3(PO_4)_2(P_2O_7)$, M = (Mn, Co, Ni), were taken at room temperature by using a Siemens D-500 diffractometer in the step scan mode, Cu Kα ($\lambda = 1.5406$ Å) radiation, at a step value of 0.02°, measuring for 20 s at each step.

The well-crystallized powders were single phases because the X-ray powder patterns of the bulk products were indexed in an orthorhombic cell (Table 2) in agreement with the parameters obtained from the single-crystal study.

(4) *International Tables for Crystallography*; Kynoch Press: Birmingham, U.K., 1974; Vol. 4, p 72.

(5) Siemens. *SAINT. Data Collection and Procedure Software for the SMART System*; Siemens Analytical X-ray Instruments, Inc.: Madison, WI, 1995.

(6) Siemens. *SHELXTL*^{TL}, version 5.0; Siemens Analitical X-ray Instruments, Inc.: Madison, WI, 1995.

(7) Dowty, E. *ATOMS for Windows 3.1, A Computer Program for Displaying Atomic Structure*; Kingsport, TN, 1995.

Table 2. X-ray Powder Diffraction Data for $Na_4M_3(PO_4)_2(P_2O_7)$ (M = Mn, Co, Ni)

hkl	phase	d_{cal} (Å)	d_{obs} (Å)	$100I/I_0$
222	Mn	2.697	2.699	100
	Co	2.644	2.648	75
	Ni	2.639	2.636	95
620	Mn	2.613	2.610	84
	Co	2.604	2.605	100
	Ni	2.594	2.594	100
200	Mn	8.993	8.984	75
	Co	9.021	9.089	57
	Ni	9.010	9.053	42
312	Mn	2.805	2.823	54
	Co	2.767	2.767	60
	Ni	2.754	2.754	75
420	Mn	3.444	3.446	53
	Co	3.415	3.412	49
	Ni	3.409	3.401	50
411	Mn	3.519	3.513	52
	Co	3.490	3.503	25
	Ni	3.487	3.482	18
011	Mn	5.655	5.660	42
	Co	5.545	5.552	35
	Ni	5.510	5.539	44
621	Mn	2.431	2.436	30
	Co	2.417	2.417	48
	Ni	2.408	2.407	38
031	Mn	3.321	3.162	30
	Co	3.263	3.078	34
	Ni	3.246	3.016	32
002	Mn	3.321	3.320	25
	Co	3.263	3.270	36
	Ni	3.246	3.238	35

Magnetic Measurements. Magnetic susceptibility was measured using a Quantum Design MPMS-XL SQUID magnetometer operating from 300 to 2 K at 500 Oe.

Ionic Conductivity. Impedance measurements were carried out in a frequency response analyzer Solartron 1174 coupled to an electrochemical interface Solartron 1286. The frequency range was $1-10^5$ Hz. In some particular cases, where the impedances were lower than 10^6 Ω, an impedance/grain-phase analyzer Solartron 1260 was used. The frequency range was $5-1 \times 10^6$ Hz. Pellets of ca. 10-mm diameter and 1.9-mm thickness were prepared from the powder samples by cold pressing at 110 MPa followed by sintering at 600 °C for 24 h. Platinum electrodes were painted on the two faces of the pellets with a platinum paste (Engelhard 6082); then, the painted pellets were heated at 200 °C for 2 h and at 600 °C for 6 h. The impedance measurements were carried out at steady temperatures on the pellets in still air.

Results and Discussion

Crystal Structure. A summary of the fundamental crystal data is given in Table 3. Final atomic coordinates are collected in Table 4. Selected bond distances, average M−O distances, and angles are given in Table 5.

The structure of these compounds is a three-dimensional array (Figure 1) that contains three crystallographically independent transition metals in octahedral coordination, with average interatomic distances $M^{II}-O$ that decrease with the radius of the divalent cation, as shown in Table 5.

The $M(3)O_6$ octahedra are rather irregular, with the smallest and the largest distances being in the range from 2.099(10) to 2.450(9) Å for manganese and from 2.004(5) to 2.649(5) Å for the nickel compound.

The PO_4 groups show a distorted tetrahedral environment due to the corner and edge sharing between the PO_4 unit and MO_6 octahedra.[2]

The diphosphate unit is formed, as usual, by two tetrahedra, $P(3)O_4$ and $P(4)O_4$, with the O(9) as the

Table 3. Crystal Data and Structure Refinement for $Na_4M^{II}_3(PO_4)_2(P_2O_7)$ (M = Mn, Ni)

	Crystal Data	
formula	$Na_4Mn_3(PO_4)_2(P_2O_7)$	$Na_4Ni_3(PO_4)_2(P_2O_7)$
formula wt (g/mol)	620.66	631.97
crystal system	orthorhombic	orthorhombic
space group	$Pn2_1a$	$Pn2_1a$
cell dimensions		
a (Å)	17.991(3)	17.999(2)
b (Å)	6.648(1)	6.4986(6)
c (Å)	10.765(2)	10.4200(9)
Z	4	4
V (Å^3)	1287.6(3)	1218.9(2)
ρcalcd (g/cm^3)	3.20	3.44
μ (mm^{-1})	3.62	5.35
dimensions	0.08 × 0.04 × 0.02	0.16 × 0.34 × 0.90
	Data Collection	
radiation	MoK$_\alpha$(λ=0.71069 Å)	MoK$_\alpha$(λ=0.71069 Å)
temp (K)	298	298
diffractometer	Siemens Smart-CCD	Siemens Smart-CCD
limiting indices	(−19,−11,−7) to (10,3,6)	(−20,−11,−7) to (16,11,6)
θ range for data collected	2.20−23.28°	2.26−23.28°
reflections collected	2744	4521
independent reflections	1501	1544
	Agreement Factors	
R	0.050	0.036
Rw	0.124	0.099

bridging oxygen and the P−O_{bridge} distances similar to those observed in previously reported diphosphates.[8]

The structure of $Na_4M_3(PO_4)_2(P_2O_7)$ (M = Mn, Co, Ni) can be described as formed by $(M_3P_2O_{13})_\infty$ blocks parallel to the *bc* plane built up from MO_6 octahedra and PO_4 tetrahedra. The blocks are connected along the *a* axis by diphosphate groups (Figure 1). Along the [100], [010], and [001] directions the polyhedral connectivity between MO_6 octahedra, PO_4 tetrahedra, and P_2O_7 diphosphates produce large tunnels where the sodium ions are located. The tunnels are intersected, giving rise to a complex three-dimensional channel system.

Magnetic Properties. The results of magnetic susceptibility measurements in the temperature range 2−300 K for $Na_4M_3(PO_4)_2(P_2O_7)$ where M = Mn, Co, Ni are plotted in Figure 2.

The temperature dependence of the magnetic susceptibility (χ), the reciprocal magnetic susceptibility (χ^{-1}), and the product χT for $Na_4Mn_3(PO_4)_2(P_2O_7)$ are shown in Figure 2. At temperatures between 30 and 275 K, the magnetic susceptibility for $Na_4Mn_3(PO_4)_2(P_2O_7)$ follows the Curie−Weiss law [$\chi^{-1} = 3.24(2) + 0.0860(2)$ T] ($r = 0.9999$), with $C = 11.62$ emu/mol Oe and $\theta = -36.5$ K. From the equation, $\mu_{eff} = (8\chi T)^{1/2}$, one obtains the effective magnetic moment per metal atom, $\mu_{eff} = 5.57\ \mu_B$. This value agrees with the magnetic moments reported for Mn(II) in others compounds (5.2−5.9 μ_B).[9] The continuous decrease in the χT values when the temperature decreases suggests antiferromagnetic exchange couplings. However, the χT curve exhibits a maximum at about 6 K that could be attributed to the existence of a ferromagnetic component, as observed in other compounds.[10]

Table 4. Atomic Coordinates for $Na_4M_3(PO_4)_2(P_2O_7)$ (M = Mn, Ni) and Equivalent Isotropic Displacement Parameters (Å^2 × 10^3) Obtained by Single-Crystal X-ray Diffraction

atom	phase	x	y	z	U(eq)[a]
M(1)	Mn	0.3411(1)	0.1010(4)	0.5049(5)	13(1)
	Ni	0.3312(1)	0.0949(2)	0.5044(1)	8(1)
M(2)	Mn	0.1413(1)	−0.4110(4)	0.4849(5)	15(1)
	Ni	0.1386(1)	−0.4158(2)	0.4955(1)	7(1)
M(3)	Mn	0.2410(1)	0.3216(4)	0.7436(4)	12(1)
	Ni	0.2404(1)	0.3197(2)	0.7443(1)	7(1)
P(1)	Mn	0.30005(2)	−0.4091(6)	0.5061(5)	10(1)
	Ni	0.2900(1)	−0.4119(4)	0.5023(2)	6(1)
P(2)	Mn	0.1797(2)	0.0825(6)	0.4834(9)	11(1)
	Ni	0.1795(1)	0.0782(4)	0.4888(2)	6(1)
P(3)	Mn	0.5638(2)	0.4603(6)	0.7296(8)	10(1)
	Ni	0.5706(1)	0.4433(4)	0.7340(2)	9(1)
P(4)	Mn	0.4468(2)	0.1546(5)	0.7539(1)	10(1)
	Ni	0.4497(1)	0.1326(4)	0.7279(2)	11(1)
Na(1)	Mn	0.4920(3)	0.8058(9)	0.9798(7)	16(1)
	Ni	0.4939(2)	0.8079(6)	0.9733(3)	16(1)
Na(2)	Mn	0.2905(3)	−0.1616(9)	0.7554(7)	21(1)
	Ni	0.2964(2)	−0.1580(6)	0.7486(3)	19(1)
Na(3)	Mn	0.3998(3)	−0.5600(10)	0.2640(8)	27(2)
	Ni	0.3897(2)	−0.5896(7)	0.2621(3)	19(1)
Na(4)	Mn	0.4650(3)	−0.3173(11)	0.5452(3)	26(1)
	Ni	0.4606(2)	−0.3400(6)	0.5404(3)	23(1)
O(1)	Mn	0.2422(4)	−0.4451(14)	0.6105(3)	12(2)
	Ni	0.2330(3)	−0.4493(8)	0.6135(5)	10(1)
O(2)	Mn	0.3555(5)	−0.5827(14)	0.4879(8)	12(2)
	Ni	0.3402(3)	−0.5944(9)	0.4753(6)	11(1)
O(3)	Mn	0.3434(4)	−0.2148(15)	0.5366(7)	10(2)
	Ni	0.3372(3)	−0.2225(10)	0.5371(5)	13(1)
O(4)	Mn	0.2512(4)	−0.3902(7)	0.3872(5)	15(2)
	Ni	0.2369(3)	−0.3806(9)	0.3852(5)	9(1)
O(5)	Mn	0.2289(4)	0.1030(15)	0.6012(1)	16(2)
	Ni	0.2369(3)	0.1035(9)	0.6062(5)	7(1)
O(6)	Mn	0.1259(5)	−0.0945(6)	0.5004(4)	19(2)
	Ni	0.1266(3)	−0.1029(9)	0.5156(5)	13(1)
O(7)	Mn	0.2383(4)	0.0499(14)	0.3790(9)	15(2)
	Ni	0.2257(3)	0.0451(8)	0.3757(5)	10(1)
O(8)	Mn	0.1367(4)	0.2745(15)	0.4503(8)	15(2)
	Ni	0.1354(3)	0.2739(9)	0.4559(6)	12(1)
O(9)	Mn	0.4817(4)	0.3776(14)	0.7085(6)	16(2)
	Ni	0.4895(3)	0.3527(9)	0.6960(5)	12(1)
O(10)	Mn	0.5558(4)	0.5594(15)	0.8540(0)	18(2)
	Ni	0.5602(3)	0.5521(9)	0.8607(5)	13(1)
O(11)	Mn	0.6176(5)	0.2870(15)	0.7561(4)	12(2)
	Ni	0.6258(3)	0.2685(10)	0.7408(5)	11(1)
O(12)	Mn	0.5800(4)	0.6141(16)	0.6274(5)	16(2)
	Ni	0.5854(3)	0.5928(10)	0.6259(5)	15(1)
O(13)	Mn	0.4655(4)	0.0933(16)	0.8615(6)	16(2)
	Ni	0.4536(3)	0.1037(9)	0.8723(5)	11(1)
O(14)	Mn	0.3640(3)	0.1739(9)	0.7088(4)	19(2)
	Ni	0.3708(3)	0.1581(9)	0.6830(5)	12(1)
O(15)	Mn	0.4814(3)	−0.0238(16)	0.6318(9)	23(2)
	Ni	0.4909(3)	−0.0032(10)	0.6475(5)	13(6)

The plot of χ^{-1} versus T (Figure 2) for $Na_4Co_3(PO_4)_2(P_2O_7)$ can also be fitted to a Curie−Weiss law [$\chi^{-1} = 4.0(1) + 0.1164(9)$ T] ($r = 0.9999$) at temperatures between 30 and 275 K. Hence, $C = 8.59$ emu /mol Oe and $\theta = -34.2$ K. By using the expression mentioned, we have obtained the effective magnetic moment per metal atom, $\mu_{eff} = 4.79\ \mu_B$, which is considerably higher than the reported spin-only value of 3.87 μ_B. The effective magnetic moments for Co(II) compounds around room temperature are between 4.4 and 5.2 μ_B[9] because of the orbital contribution. Therefore, the magnetic moment of $Na_4Co_3(PO_4)_2(P_2O_7)$ could be due to this contribution. The negative θ value together with the continuous decrease of the χT values with decreasing

(8) Sanz, F.; Parada, C.; Ruíz-Valero, C. *Chem. Mater.* **2000**, *12*, 671.

(9) Carlin, R. L. *Magneto-Chemistry;* Springer-Verlag: New York, 1986.

(10) Goñi, A.; Lezama, L.; Moreno, N. O.; Fournès, L.; Olazcuaga, R.; Barberis, G. E.; Rojo T. *J. Magn. Magn. Mater.* **2000**, *12*, 62.

Table 5. Selected Interatomic Distances and Average M−O Distances (Å) and Angles (°) for $Na_4M_3(PO_4)_2(P_2O_7)$ (M = Mn, Co, Ni)[a]

distances	Mn	Co	Ni
M(1)−O(3)	2.127(10)	2.070(5)	2.093(6)
M(1)−O(5)	2.269(8)	2.127(4)	2.073(5)
M(1)−O(7)	2.318(9)	2.279(5)	2.204(5)
M(1)−O(14)	2.285(9)	2.108(5)	2.034(5)
M(1)−O(2^1)	2.217(10)	2.109(5)	2.048(5)
M(1)−O(12^2)	2.159(8)	2.040(5)	2.024(5)
M(2)−O(1)	2.278(8)	2.153(5)	2.109(5)
M(2)−O(4)	2.244(8)	2.175(5)	2.122(5)
M(2)−O(6)	2.128(11)	2.096(6)	2.055(6)
M(2)−O(8^3)	2.126(10)	2.047(6)	2.059(6)
M(2)−O(10^4)	2.174(8)	2.106(5)	2.069(5)
M(2)−O(13^5)	2.340(8)	2.178(4)	2.101(5)
M(3)−O(5)	2.123(9)	2.013(5)	2.016(5)
M(3)−O(14)	2.450(9)	2.538(5)	2.649(5)
M(3)−O(1^1)	2.110(9)	2.078(5)	2.033(5)
M(3)−O(11^6)	2.235(9)	2.202(5)	2.096(6)
M(3)−O(4^7)	2.099(10)	1.993(5)	2.004(5)
M(3)−O(7^7)	2.138(9)	2.100(5)	2.051(5)

average distances	Mn	Co	Ni
M(1)−O	2.229(7)	2.122(6)	2.079(8)
M(2)−O	2.215(0)	2.126(5)	2.086(3)
M(3)−O	2.193(2)	2.154(5)	2.142(0)
Na(1)−O	2.387(11)	2.382(6)	2.384(7)
Na(2)−O	2.536(10)	2.503(6)	2.481(7)
Na(3)−O	2.670(10)	2.659(6)	2.552(7)
Na(4)−O	2.587(10)	2.581(6)	2.586(7)

angle	Mn	Co	Ni
M(3)−O(1)−M(2)	117.9(4)	119.6(3)	121.3(2)
M(3)−O(4)−M(2)	116.5(4)	127.0(4)	129.6(3)
M(3)−O(5)−M(1)	104.0(4)	107.7(2)	108.8(2)
M(3)−O(7)−M(1)	111.3(3)	109.4(3)	110.3(2)
M(1)−O(14)−M(3)	93.9(3)	91.5(2)	89.4(2)

[a] Symmetry code: (1) (x, $1 + y$, z); (2) ($1 - x$, $y - 1 - 1/2$, $1 - z$); (3) (x, $y - 1$, z); (4) ($x - 1/2$, $y - 1$, $-z + 2 + 1/2$); (5) ($1/2 - x$, $y - 1/2$, $z - 1/2$); (6) ($x - 1/2$, y, $1 + 1/2 - z$); (7) ($1/2 - x$, $1/2 + y$, $1/2 - z$).

temperature indicate that the main Co^{II} interactions are antiferromagnetic.

The upward deviations from the Curie−Weiss behavior at lower temperatures can be due to two different causes.[9] Cobalt(II) with three unpaired electrons exhibits an important orbital contribution at high temperatures with a spin−orbit contribution coupling constant of $\lambda = 180$ cm^{-1}. This phenomenon produces the depopulation of the higher energy level associated with the $^4T_1$ ground state, giving rise to the decrease in the susceptibility values. But also the deviations can be attributed to the onset of antiferromagnetic interactions. The spin−orbit coupling causes an effect qualitatively similar to that originating from the antiferromagnetic interactions and both contributions in our case are more important than the zero-field splitting.

A careful analysis of the χ versus T plots in Figure 2, corresponding to the manganese and cobalt compounds, shows an inflection point at about 6 K, which also seems to indicate the presence of a ferromagnetic component.

Concerning the temperature dependence of χ for the nickel compound, χ increases upon cooling, showing a maximum at 12 K (Figure 2). This result together with the continuous decrease in $t\,\chi T$ upon decreasing temperature are an indication of antiferromagnetic ordering of Ni^{II} ions. The data above 40 K were least-squares fitted to a Curie−Weiss equation [$\chi^{-1} = 4.8(7) +$ 0.26298(7) T] ($r = 0.99999$), with $C = 3.84$ emu/mol Oe and $\theta = -18.1$ K. The calculated magnetic moment per metal atom was 3.20 μ_B, which agrees with the experimental reported moments for other nickel(II) compounds (2.9−3.4 μ_B).[9]

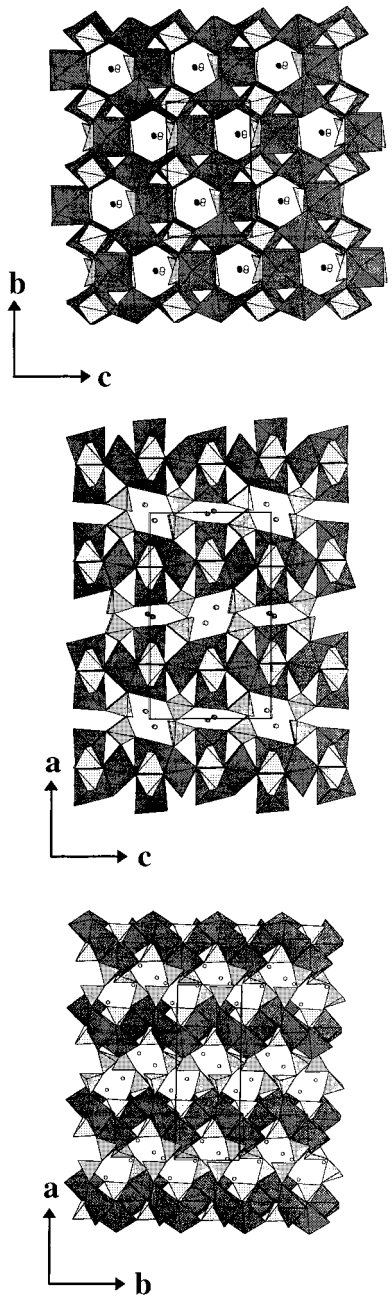

Figure 1. Polyhedral view along the [100], [010], and [001] directions of $Na_4M_3(PO_4)_2(P_2O_7)$ (M = Mn, Co, Ni) structure, showing the three channels where Na cations are located.

Figure 3 shows the field dependence of the magnetization for the three compounds at different temperatures. In these measurements, the field has been increased and then decreased, as indicated by the arrows. For the manganese compound a change in the slope of the curve at 5 and 2 K can be observed. The value of the extrapolated moment is obtained by projecting the high-field slope to $H = 0$ in Figure 3. The values of the moments extrapolated for the manganese compound, at 5 and 2 K, are about 0.7and 0.9 μ_B, respectively. On the other hand, in the case of $Na_4Co_3(PO_4)_2(P_2O_7)$ the curve registered at 2 K is not retraced

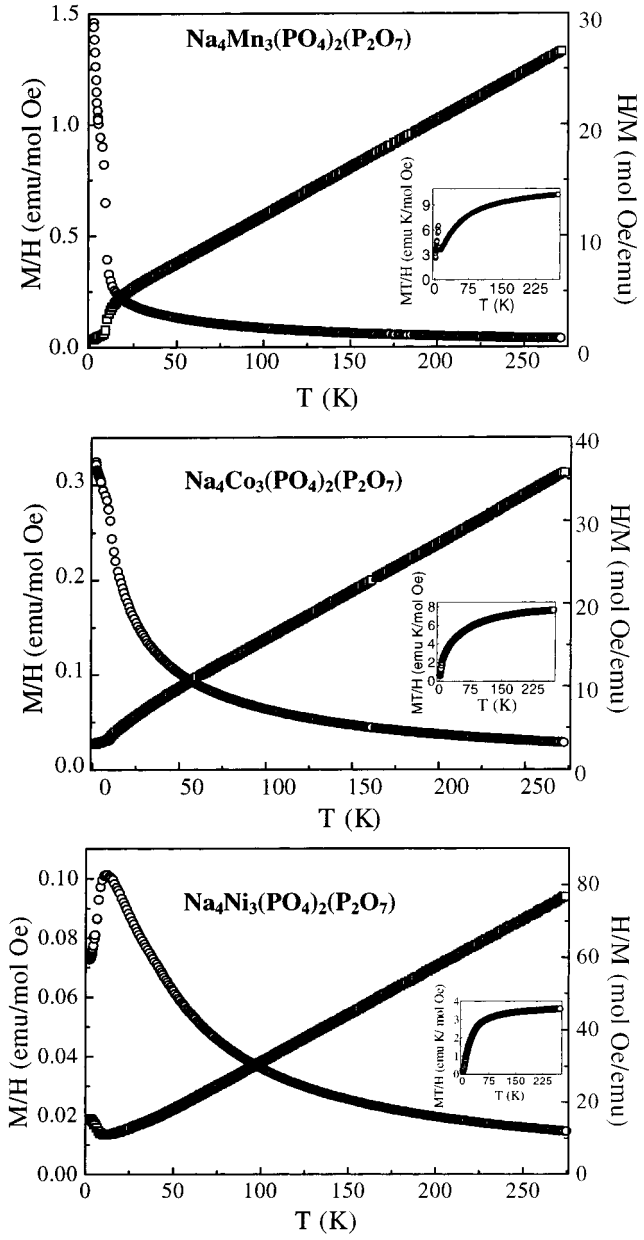

Figure 2. Magnetic susceptibility (χ, open circles) and inverse magnetic susceptibility ($1/\chi$, open squares) plotted as a function of temperature for powder samples of $Na_4Mn_3(PO_4)_2(P_2O_7)$, $Na_4Co_3(PO_4)_2(P_2O_7)$, and $Na_4Ni_3(PO_4)_2(P_2O_7)$. The insets show the thermal evolution of the χT product for these three phases.

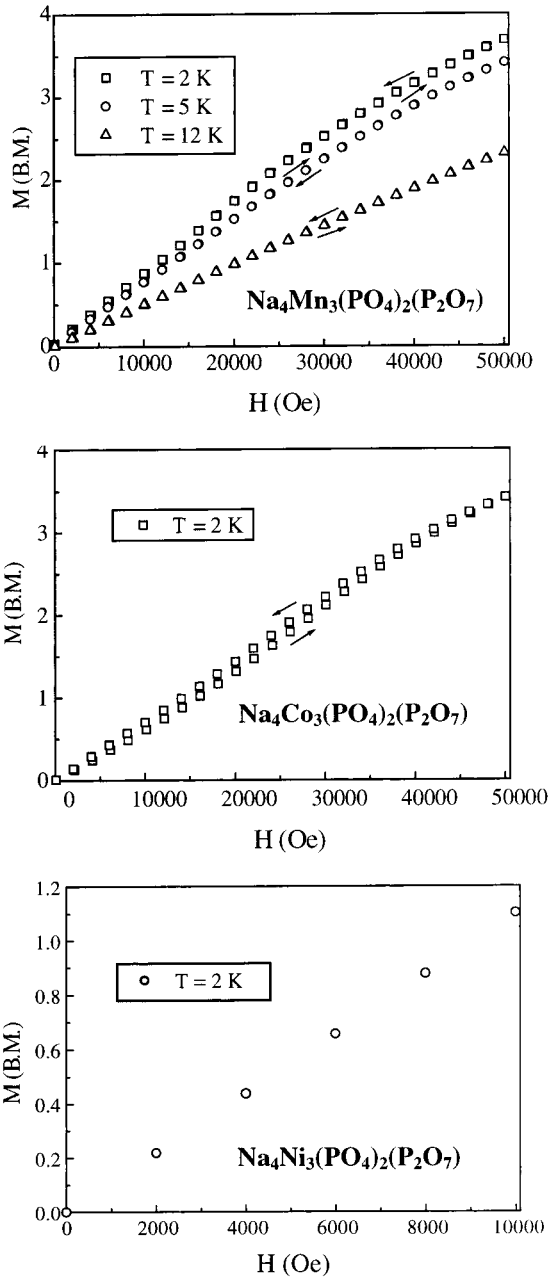

Figure 3. *M* vs *H* plots with the magnetic field increased and decreased (see arrows) at different temperatures for $Na_4Mn_3(PO_4)_2(P_2O_7)$, $Na_4Co_3(PO_4)_2(P_2O_7)$, and $Na_4Ni_3(PO_4)_2(P_2O_7)$.

and exhibits a small hysteresis loop (Figure 3). These results of the magnetization versus field for manganese and cobalt compounds also indicate the presence of a weak ferromagnetic component that could be explained by slight canting of the magnetic moments. In the nickel compound, the *M*(*H*) behavior shows a straight line at 2 K, which is typical of antiferromagnetic behavior.

The magnetic coupling between two adjacent metal centers in these phosphates can be through −O−P−O− bridges or −O− bridges.[11] Considering the structural features exhibited by these phases, at least three different magnetic exchange pathways could be deduced (Figure 4). One of them involves the interactions through $-M(2)O_6-M(3)O_6-M(2)_6-$ zigzag chains in the [0 1 1] direction, which are built up from corner sharing between MO_6 octahedra. A second pathway implies the magnetic coupling through $-M(1)O_6-M(3)O_6-M(1)O_6-$ metallic chains in the [0 1−1] direction, which are formed by corner and edge sharing between MO_6 octahedra. Both exchange pathways would produce antiferromagnetic couplings in the subnetwork of transition metal polyhedra, which is two-dimensional from the magnetic point of view. The bond angles differ by 180°, as shown in Table 5, which indicates a poor d-orbital overlap that is consistent with the antiferromagnetic ordering observed in these compounds at lower temperatures.

Therefore, the antiferromagnetic ordering in the nickel compound and the canting antiferromagnetism observed in manganese and cobalt compounds agree with the structural features found in theses compounds

(11) Bu, X.; Feng, P.; Stucky, G. D. *J. Solid State Chem.* **1997**, *131*, 387.

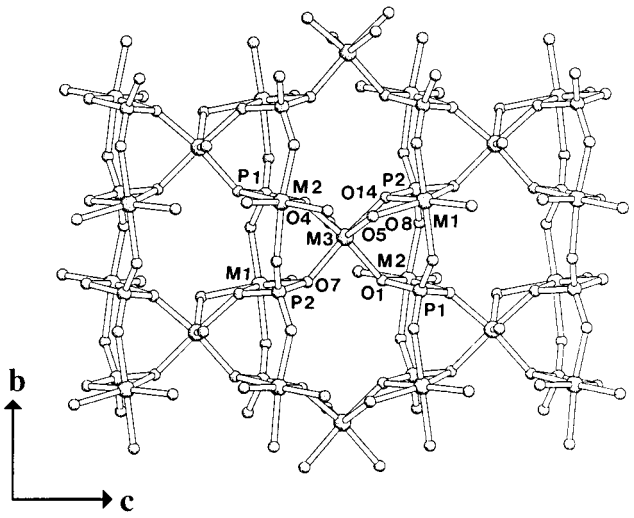

Figure 4. Representation of one $(M_3P_2O_{13})_\infty$ block showing the corner- and edge-sharing scheme between MO_6 octahedra and PO_4 tetrahedra.

with infinite M−O−M zigzag chains (Figure 4). As the illustration of the $Na_4M_3(PO_4)_2(P_2O_7)$ structure clearly shows, the octahedra along the zigzag chains are successively tilted with respect to each other. This structural condition could be a possible cause of canting of the magnetic moments in the manganese and cobalt compounds.[9]

The third exchange pathway implies the coupling between successive blocks through PO_4 groups that must be antiferromagnetic to justify the global antiferromagnetism, as has been observed for other transition metal phosphates.[12,13]

Finally, the weak value of the Néel temperature could be explained for all these facts: weak superexchange antiferromagnetic interactions through the corner- and edge-shared MO_6 octahedra, two-dimensional character of the magnetic lattice, and magnetic couplings through the PO_4 groups.

Ionic Conductivity. The impedance plots (imaginary vs real part) recorded for $Na_4Mn_3(PO_4)_2(P_2O_7)$ and $Na_4Ni_3(PO_4)_2(P_2O_7)$ are shown in Figure 5, top and bottom, respectively. The impedance plot for $Na_4Co_3(PO_4)_2(P_2O_7)$ is similar to the plot observed for the Ni compound, and in both cases the plot shows only one arc and a spike. Upon heating, the arc disappears from the plot and the inclined spike is better observed. The capacitance (C) of the spike, deduced from the ideal expression $Z'' = -1/C\omega$, where Z'' is the imaginary impedance and $\omega = 2\pi\nu$, ν being the frequency in Hz, is in the order of magnitude of 1−10 μF. The spike, which is indicative of an ionic conductor, is ascribed in our samples to blocking of Na^+ ions at the electrode surfaces. The arc is well-fitted (see the solid line) to a expression of the form $Z^* = 1/(1/R + B(i\omega)^n)$, where Z^* is the complex impedance, R is the resistance, and B and n are parameters of a universal capacitor (CPE), both R and CPE being arranged in a parallel circuit.[14] The fitting was done on the data recorded at different temperatures, and R was determined at each temperature. Then, the conductivity was calculated at each temperature as usual. The capacitance of the arc is 4 and 8 pF for the Ni and Co compound, respectively. These values are close to those usually reported for the bulk (or grain interior) response (1−10 pF).[15,16] This fact confirms that the arc observed in the impedance plot for the Ni and Co compound is due to movement of Na^+ ions within the phosphate framework. The impedance plots recorded for the Mn pellet show two arcs (Figure 5, top). These plots are fitted (see the solid line) to the expression $Z^* = Z_1^* + Z_2^*$, where Z_1^* and Z_2^*, which are the complex impedances for the two arcs, adopted the expression already mentioned for a parallel circuit of R and CPE. From the fittings done we determined the resistances associated with each arc, and then, we calculated their conductivities. The arc at high frequency shows a capacitance of 5 pF, which agrees with the capacitance reported for the bulk response. The capacitance of the arc at low frequency is 2 nF, and this value is close to the capacitance usually found for the grain boundary response,[15,16] that is, for the motion of Na^+ ions through boundaries of neighboring grains. Therefore, the high-frequency arc and the low-frequency one are ascribed to the bulk (or grain interior) and grain boundary responses, respectively. Upon heating, first

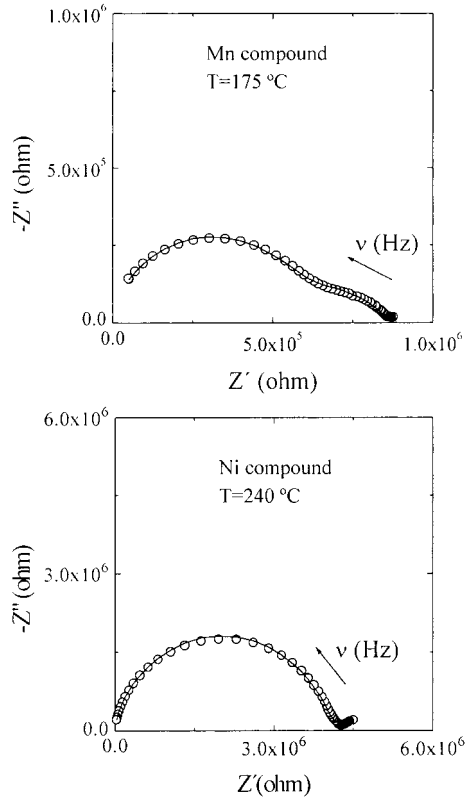

Figure 5. Impedance plots ($-Z''$ vs Z') obtained for the $Na_4Mn_3(PO_4)_2(P_2O_7)$ and $Na_4Ni_3(PO_4)_2(P_2O_7)$ compound. The solid lines stand for the best fits. The parameters are as follows: $R_1 = 5.6 \times 10^5$ Ω, $B_1 = 2.5 \times 10^{-11}$, $n_1 = 0.93$, $R_2 = 3.0 \times 10^5$ Ω, $B_2 = 1.2 \times 10^{-8}$, $n_2 = 0.65$ for the Mn pellet and $R = 4.2 \times 10^6$ Ω, B(CPE) $= 1.7 \times 10^{-11}$, n(CPE) $= 0.92$ for the Ni one.

(12) Lezama, L.; Suh, K. S.; Villenueve, G.; Rojo, T. *Solid State Commun.* **1990**, *76*, 449.
(13) Goñi, A.; Lezama, L.; Barberis, G. E.; Pizarro, J. L.; Arriortua, M. I.; Rojo T. *J. Magn. Magn. Mater.*, **1996**, *164*, 251.
(14) Jonscher, A. K. *Dielectric Relaxation in Solids;* Chelsea Dielectric: London, 1983.
(15) Ross Macdonald, J. *Impedance Spectroscopy. Emphasizing Solid Materials and Systems;* John Wiley & Sons: New York, 1987.
(16) Irvine, J. T. S.; Sinclair, D. C.; West, A. R. *Adv. Mater.* **1990**, *2−3*, 132.

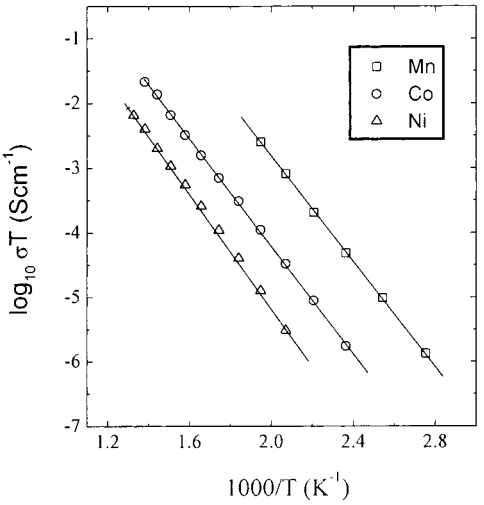

Figure 6. Plot of the bulk conductivity (open symbols) vs 1000/*T* for the Mn, Co, and Ni compound. The straight lines are the best fits to the equation $\sigma T = \sigma_0 \exp(-E/KT)$.

Table 6. Activation Energies (*E*), Pre-exponential Factors (σ_0), and Ionic Conductivity at 330 °C (σ_{300}) for $Na_4M_3(PO_4)_2(P_2O_7)$ (M = Mn, Co, Ni)

compound	*E* (eV)	σ_0 (S cm^{-1})	σ_{300} (S cm^{-1})
$Na_4Mn_3(PO_4)_2(P_2O_7)$	0.81 ± 0.01	$2.1 \pm 0.3 \times 10^5$	2.7×10^{-5}
$Na_4Co_3(PO_4)_2(P_2O_7)$	0.82 ± 0.01	$1.2 \pm 0.1 \times 10^4$	1.3×10^{-6}
$Na_4Ni_3(PO_4)_2(P_2O_7)$	0.86 ± 0.02	$5.4 \pm 0.9 \times 10^3$	2.1×10^{-7}

the high-frequency arc and then the low-frequency one disappear gradually from the plot while the spike is better observed.

The plot of the bulk conductivity (log(σT)) vs reciprocal temperature (1000/*T*) is shown in Figure 6 for the three compounds. The data are well-fitted to the Arrhenius expression $\sigma T = \sigma_0 \exp(-E/KT)$, where σ_0 is a pre-exponential factor, *E* is the activation energy, and *K* is the Boltzmann constant. The *E* and σ_0 parameter, together with the conductivity at 300 °C, are outlined in Table 6. *E* is similar for the three compounds (0.81−0.86 eV). However, σ at 300 °C increases from 2.1×10^{-7} S cm^{-1} for the Ni compound to 2.7×10^{-5} S cm^{-1} for the Mn one. The increase in conductivity of 2 orders of magnitude is associated with the rise in σ_0. This can be related to an increase in the dimensionality of the Na^+ ion conduction. To check this point, conductivity measurements along the three crystallographic axes should be done. However, the lack of single crystals of sufficient size prevented us from obtaining such experimental evidence.

We have estimated the average Na−O distances for the four crystallographically different Na^+ ions and we have analyzed how they are arranged in the tunnels. According to the structure, a complex scheme of tunnel intersections gives rise to the formation of a three-dimensional channel network that hosts the sodium cations.[2] The Na(1) and Na(4) atoms are placed along the B2 and B1 tunnels, respectively, both (B1 and B2) running parallel to the *b* axis. These tunnels intersect with another kind of tunnel (C1) running parallel to the *c* axis. The Na(1) and Na(4) atoms are placed at the intersection of B2 and C1 and B1 and C1, respectively. This produces a two-dimensional channel system parallel to the *bc* plane and is located between two neighboring $(Co_3P_2O_{13})_\infty$ blocks. There is another kind of tunnel (A1) running parallel to the *a* axis. In this tunnel the Na(2) and Na(3) ions are placed in an alternating way; Na(2) is located at the height of the $(Co_3P_2O_{13})_\infty$ sheet, and Na(3) is placed at the intersection of the A1 tunnel with the C1 one. Therefore, Na^+ ion conduction must involve Na(1) and Na(4) if that occurs in the *bc* plane and Na(2) and Na(3) if that occurs along the *a* axis.

The average Na−O distances for the four kinds of Na^+ ions in the Mn, Co, and Ni compound are shown in Table 5. The Na(1)−O and Na(4)−O distances are very close for the three compounds, suggesting that the Na^+ ion motion in the *bc* plane is similar in the three cases. However, the Na(2)−O and Na(3)−O distances increase gradually from the Ni compound to the Mn one. It should favor motion of the Na^+ ions along the *a* axis, and hence, it points to an increase in the dimensionality of the ionic conduction.

Acknowledgment. This work was supported by the Spanish CICYT and DGICYT under Projects MAT98-0920, MAT98-1735, and PB97-1200. We thank the staff of C.A.I. de Espectroscopia de Plasma, U.C.M., for chemical analysis. We express our gratitude to Prof. J. L. Martinez for the magnetic measurements and Prof. I. Rasines for fruitful comments and discussion.

CM001210D